Spectrochimica Acta Part B 113 (2015) 152–157

Contents lists available at ScienceDirect

Spectrochimica Acta Part B

journal homepage: www.elsevier.com/locate/sab

Time-resolved line emission spectroscopy and the electrical currents in the plasma jet generated by dielectric barrier discharge for soft ionization

Vlasta Horvatic [a,*], Antje Michels [b], Norman Ahlmann [b], Günter Jestel [b], Cedomil Vadla [a], Joachim Franzke [b]

[a] Institute of Physics, Bijenicka 46, 10000 Zagreb, Croatia
[b] ISAS-Leibniz Institut für analytische Wissenschaften, Bunsen-Kirchhoff-Str. 11, 44139 Dortmund, Germany

ARTICLE INFO

Article history:
Received 20 May 2015
Accepted 22 September 2015
Available online 30 September 2015

Keywords:
Dielectric-barrier-discharge ionization
Soft ionization
Time-resolved emission spectroscopy

ABSTRACT

The spatially and temporally resolved optical emission from the helium capillary dielectric barrier discharge driven by a square wave high voltage was measured simultaneously with the discharge currents during the positive and negative voltage periods. The He and N_2^+ emission intensities were monitored at 501 nm and 391 nm, respectively. The plasma jet was found to be formed only during the positive voltage period, and it preceded the discharge ignition in the capillary. Thus, the measurements of the difference between the capillary discharge currents during the positive and negative voltage periods enabled quantification of the charge, which was transported through the plasma jet. The analysis of the spatiotemporal behavior of the He emission intensities in the plasma jet yielded the velocity of the helium excitation propagation and the effective plasma jet length. The combination of these measurements enabled determination of the absolute values of the plasma jet currents. The linear relationship between the He emission intensities in the plasma jet and the plasma jet currents was found to exist over the emission intensity range of two orders of magnitude. The N_2^+ emission intensity was also found to be linearly dependent on the plasma jet current. The fast electrons, producing the excited He atoms, were found to be located mostly within the estimated effective plasma jet length. In this region a cascade of processes involving excited He atoms, N_2^+ and H_2O molecules lead to establishment of the conditions necessary for the plasma jet to be used as soft ionization source. The production of reactive species can be related to the plasma jet current, which can serve as a measure of the soft ionization efficiency.

1. Introduction

Nowadays, mass spectrometry can be regarded as one of the most widely used and useful analytical methods. It requires ionized species as an input, and except for the intrinsically charged analytes, the investigated samples have to be ionized. A necessity for real time or *in situ* sample monitoring resulted with the need to ionize species outside the mass spectrometer inlet and to use a sample with little or no preparation at all. Dielectric barrier discharges (DBDs) have manifested themselves as flexible and practical ionization sources which meet all these requirements. Moreover, DBDs have additional favorable features like high dissociation ability at low working temperature and low power consumption [1], operation with a variety of gases at low flow rates and versatile geometry [2], which make them attractive as a base for construction of variety of analytical devices. Recent reviews [2–4] summarize the basics of DBD operation, their development and the potential for future applications. Due to their favorable characteristics, a number and diversity of DBDs applications have extended beyond the molecular mass spectrometry [5–8]. They have been used in many different scientific and technological areas, such as gas chromatography [9,10], ion mobility spectrometry [11,12], atomic fluorescence and diode laser spectrometry [13,14], element-selective detection [1], forensics [15,16], *in vivo* analysis [17–19], plasma cleaning [20,21], ozone generation for disinfecting water [22] and surfaces [23], pesticide testing [24], as light sources [25,26], and as sources for atomic emission spectroscopy [27,28].

The most important part of the capillary DBD for its use as ionization source is the plasma jet formed at the capillary exit, which protrudes in the surrounding atmosphere. The extensive investigations of the dynamics and the formation process of the DBD jet [29–35] lead to interpretation that the jet is formed in a streamer like manner subsequent to the discharge in the capillary, and that it propagates in the form of so called plasma bullets. However, there are two investigations [30,35], which indicated that the jet is formed independent of and prior to the discharge in the capillary. The detailed spatial and temporal investigation of this phenomenon has been reported recently [36,37].

The measurements in Refs. [36,37] were related to the plasma in the capillary due to the discharge between the electrodes, so called electrode plasma, as well as to the plasma jet, which is essential for the soft ionization. During these investigations, various electrode configurations were used. In the optimum configuration, *i.e.*, when the plasma jet

* Corresponding author.
E-mail address: blecic@ifs.hr (V. Horvatic).

http://dx.doi.org/10.1016/j.sab.2015.09.017
0584-8547/

is the brightest and the longest, the front electrode near the capillary orifice was connected to the AC high voltage (HV) output, while the rear electrode was connected to the ground. By applying the time resolved emission spectroscopy, it was found out that in the described electrode configuration, the plasma jet occurs only during the positive voltage period, while in the negative voltage period there was only a plasma in the capillary present. Furthermore, it was revealed that during the positive voltage period the plasma jet and the electrode plasma constitute two events in time. The plasma jet formed before the occurrence of the plasma current between the electrodes and the ignition of the electrode plasma.

By comparison of the effects produced by the application of a sinusoidal-like HV (SLHV) and square-wave shaped HV (SQHV) generator, it was found out that the application of the latter showed a series of advantages. First, the DBD could operate at much lower HV amplitudes than in the case of the sinusoidal one. This means that at equal HV amplitudes the SQHV produces much more intense plasma jet than the SLHV [37].

As it was shown previously [38–40], the He-DBD driven with a SLHV can be operated either in a homogeneous or filamentary mode, which can be distinguished by a single or multiple DBD current peaks during one voltage duty cycle, respectively. In contrast to the case of SLHV, the He-DBD operates in the homogeneous mode in a wide range of the SQHV amplitudes with no jumps to filamentary mode.

Besides the mentioned advantages, the application of the SQHV yields a possibility to get a better insight into the processes, which lead to the formation of both the electrode plasma and the plasma jet. When applying an AC high voltage, the current through the capillary consists of two components. The first one is the displacement current due to the polarization of the dielectric material, which is in contact with the electrodes, and due to the polarization of the gas between the electrodes. The second current component corresponds to the discharge ignition and formation of the plasma in the capillary. The displacement current is proportional to the time derivative of the applied voltage ($I_{disp} \propto dV(t)/dt$), and in the case of SLHV it flows continuously [36], thus it is difficult to draw any quantitative conclusions from the comparison of the positive and negative current signals. In the case of SQHV the displacement current has a form of a sharp peak matching the voltage rising and falling edges. In this case the corresponding discharge currents yield important information, which will be presented in the following.

As shown previously [37], the comparison of the plasma currents during the positive and negative period yields the opportunity to quantify the charge, which is transported through the plasma jet. The present investigation will show that by the determination of this charge in combination with the time resolved measurements of the excited helium line intensities in the plasma jet the absolute values of the plasma jet current can be obtained. They can be directly related with line emission intensities in the jet and also used as a measure for the soft ionization efficiency. As the representative for He optical emission, the line at 501 nm was chosen. Simultaneously, the presence of ionized nitrogen was controlled. The ionized nitrogen molecule is commonly accepted as crucial for water protonation and subsequent soft ionization of large molecular samples. For that reason the transient emission signals of N_2^+ at 391 nm, corresponding to the head of the N_2^+ B-X band, were measured.

2. Experimental section

2.1. Experiment

The experimental arrangement and the type of the capillary DBD were the same as in our recent work [37] and it will be only briefly described. The inner and outer radii of the used glass tube were 0.5 and 1 mm, respectively. The front electrode was connected to the SQHV generator (frequency: 2 kHz, peak-to-peak voltage maximum: 3.5 kV), while the rear electrode was connected to the ground by a resistor ($R = 100\ \Omega$) in order to measure the current. The output of the current probe was fed to a two-channel 70 MHz storage oscilloscope (Agilent DSO-X 2002A). The oscilloscope was working in the averaging mode and triggered by a sharp displacement current peak. The measurements were performed at constant He flow trough the capillary (0.5 SL/min), while the SQHV amplitude was varied from 2.4 to 3.5 kV. The He (501 nm) and N_2^+ (391 nm) optical emission from the plasma in the capillary and in the jet was observed at right angles with respect to the discharge axis x and detected by a system comprising a 1 m McPherson monochromator, an EMI 9789 photomultiplier and a home-made fast amplifier. Two pairs of signals were measured. Simultaneously with the current, either HV or the photomultiplier amplifier (rise time: 0.8 ns) output was monitored by 70 MHz digital storage oscilloscope triggered by the current signal. The current probe of the Agilent DSO-X 2002A oscilloscope was used to measure the voltage over a 100 Ω metal film resistor. In order to prevent the storage oscilloscope against damage an over voltage protection G31A75 was set parallel to the resistor. The sketch of the DBD configuration and the typical current signals for two different square-wave HV amplitudes are displayed in Fig. 1.

2.2. Measurements

The transient line emission signals of the He 501 nm and N_2^+ 391 nm lines were measured stepwise (steps: 1 mm) along the DBD x-axis with a spatial resolution $dx = 0.3$ mm. The origin of the x scale was set to the right edge of the rear electrode and the measurements were performed from the middle of the capillary ($x = 5$ mm) over the front HV electrode (right edge: $x = 10$ mm) up to $x = 22$ mm in the plasma jet. As reported in our previous investigations [36,37], during the positive and negative voltage periods there are strong He emission signals in the capillary between the electrodes, which coincide with the positive and negative peaks of the discharge current. These coincident signals are negligible in the region of the plasma jet. The emission signals, which precede the plasma current ignition, occur during the positive voltage period. These so called early signals are measurable in the capillary as well as in the plasma jet region. During the negative voltage period the early signals could not be detected. Unlike previously [36,37], only the early signals will be considered here. Typical early emission signals of the He 501 nm line measured at three positions outside the capillary are shown in Fig. 2 together with the respective plasma current signals.

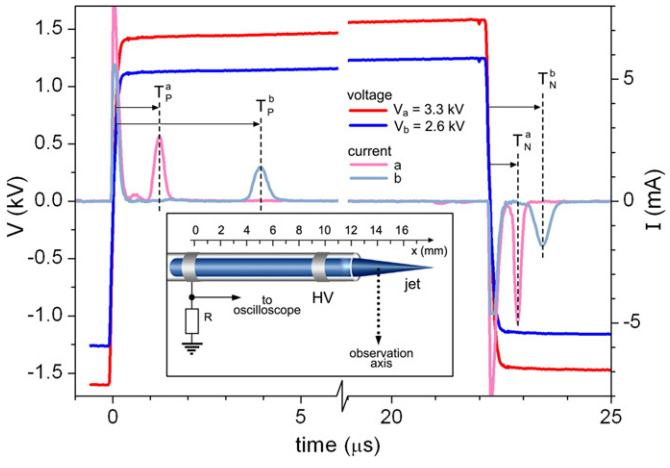

Fig. 1. Typical time-dependent discharge current signals obtained for two peak-to-peak voltage amplitudes (V_a and V_b). The T_P and T_N label the ignition times of the discharge between the electrodes for the positive and negative voltage periods with respect to the corresponding sharp displacement current peaks. Inset: schematic diagram of the DBD configuration. The electrodes are 1 mm wide and their centers are separated by 10 mm. The edge of the front electrode has a distance of 2.5 mm from the capillary orifice.

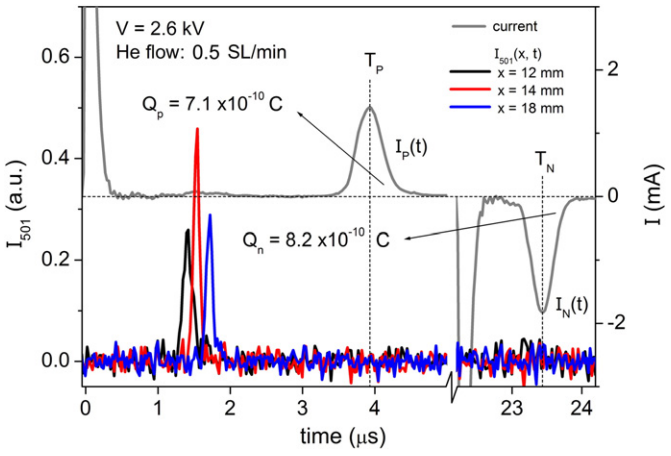

Fig. 2. Plasma current signals and early He 501 nm emission signals at three positions in the region of the plasma jet measured with the peak-to-peak SQHV amplitude of V = 2.6 kV. The areas under the plasma current signals correspond to the charges Q_P and Q_N transported through the plasma in the capillary during the positive and negative voltage period, respectively. See further comments in the text.

Generally, in the present electrode configuration the ignition time T_P was greater than T_N. The T_P and T_N values as well as their differences decreased with increasing voltage. The areas $Q_P = \int I_P(t)\ dt$ and $Q_N = -\int I_N(t)dt$ defined by the positive $I_P(t)$ and negative $I_N(t)$ discharge current signals represent the charges transported through the capillary and their values Q_P and Q_N for positive and negative current peaks are different. In the present electrode configuration their difference $\Delta_Q = Q_N - Q_P$ was always positive. In the case when the rear electrode was connected to the HV and the front electrode was grounded, this difference was practically zero. As mentioned previously, in that case the plasma jet was negligible.

As can be seen in Fig. 2 the He 501 nm emission signals in the jet occur in the period between the positive displacement and positive plasma current. Here, we define the occurrence time as the time when the particular emission intensity reaches its maximum. Both peak intensities and occurrence times τ strongly depend on the position x. Their spatial distributions for the He 501 nm and N_2^+ 391 nm lines were measured at six different high voltage amplitudes ranging between 2.4 kV and 3.5 kV, while the helium flow was kept constant. The obtained data for the He 501 nm line are plotted in Fig. 3.

The first early signals of the He 501 line appear in the vicinity of the HV electrode (x = 9 mm and 11 mm). With increasing distance from the electrode the intensities in both +x and −x direction become larger and their occurrence on the time scale is closer to the corresponding ignition time T_P. The He intensities exhibit maxima at the capillary orifice and continuously decrease in the jet with increasing x. The reciprocal slopes dx/dτ of the τ(x) distributions yield the values for velocities v^E, which are attributed to the propagation of the excitation of He atoms. The possible explanation of the dynamics of this process was outlined in [36,37]. In the applied voltage range, the excitation velocities v_3^E in the plasma jet are much higher than the velocities v_1^E and v_2^E in the capillary near the HV electrode. As already stated previously [37], these velocities cannot be attributed to either the velocities of the excited helium atoms or the velocities of electrons responsible for their excitation. However, as it will be shown in the following, the excitation velocity can be treated as a physical observable related to the charge transport, *i.e.*, the electrical current in the plasma jet.

The data for position-dependent peak intensities and occurrence times of the N_2^+ 391 nm emission are plotted in Fig. 4. In contrast to the case of He 501 nm line, the N_2^+ early emission in the capillary is weak, and becomes strong in the jet. The $I_{391}(x)$ distributions exhibit maxima at a certain x position, which generally depends on the applied He gas flow. With increasing HV in the present range, the maximum

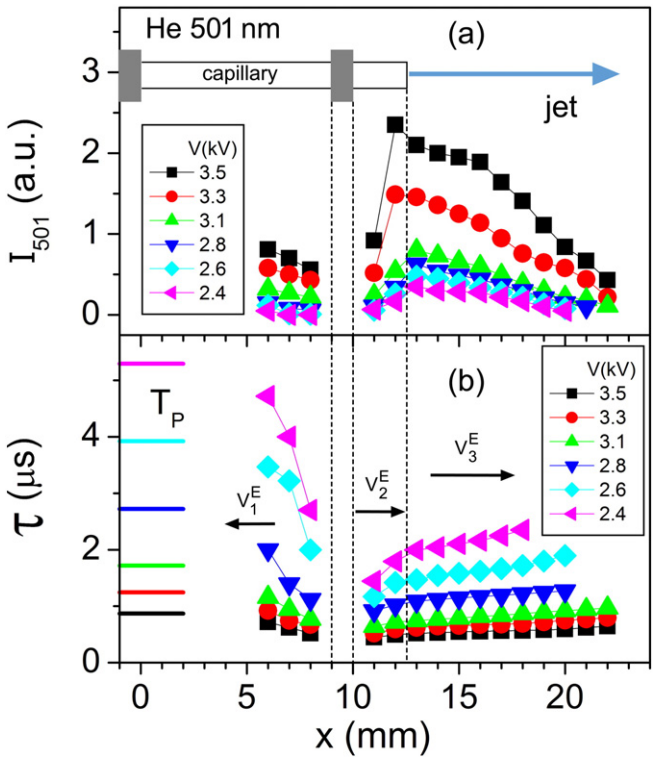

Fig. 3. (a) Position-dependent peak intensities of the early emission signals of the He 501 nm line measured at a series of applied voltages V. (b) Ignition times T_P (colored horizontal bars) and position-dependent occurrence times τ of the early He 501 nm line emission signals. The error bars are of the size of the symbols. The arrows labeled with v_n^E (n = 1, 2, 3) represent the direction of the He excitation propagation velocities. See further explanation in the text.

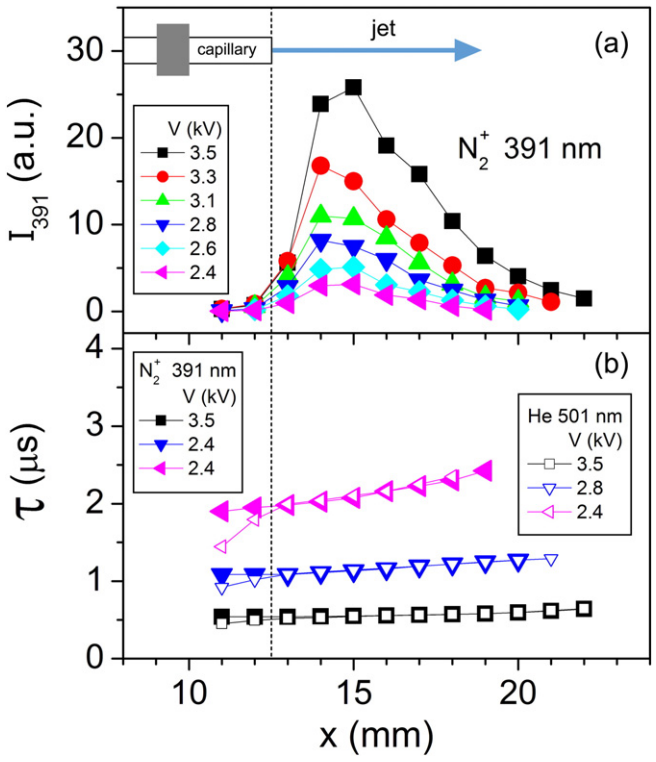

Fig. 4. (a) Position-dependent peak intensities of the early N_2^+ 391 nm emission measured at various voltages. (b) Position-dependent occurrence times of the early N_2^+ 391 nm emission compared with the He 501 nm line emission. The data for the He line are taken from Fig. 3b. For the sake of the picture clarity only the data for V = 3.5 kV, 2.8 kV and 2.4 kV are displayed. The error bars are of the size of the used symbols.

values of $I_{501}(x)$ and $I_{391}(x)$ increase strongly and in the same mutual proportions.

As for the occurrence times, the early N_2^+ 391 signals are delayed with respect to the He 501 nm signals in the region $10 < x < 13$. This is shown in Fig. 4b, where the occurrence times for N_2^+ are compared with those of He. For the sake of picture clarity, in Fig. 4b only a part of the obtained data set is displayed. In the plasma jet, the occurrence times of N_2^+ and He emission signals match each other.

As can be seen in Figs. 1 and 2 there is a small current bump preceding the ignition in the capillary at time T_P. When the HV positive slope starts and the glass is polarized so that the surface of the glass is charged positively the electrons in between the electrodes and outside the capillary will be attracted and accelerated in the direction to the positively charged glass wall under the positive electrode. Therefore, the small current between the displacement current and the current peak at T_p might be the current initiated by these electrons starting from the ground electrode in the direction to the positive charged glass surface. When the energy of these electrons is sufficiently high enough metastable He atoms will be excited. These will generate N_2^+ ions in collisions with N_2 molecules. Then a part of the peak at T_p is measured when the much slower N_2^+ ions reach the glass surface at the ground electrode.

2.3. Analysis of the measurements

The higher excited He states can be produced by electron impact form the ground state at rate R_1 or by He^+ and He_2^+ ions through ion-electron recombination and ion-electron dissociative recombination at rates R_2 and R_3, respectively. The corresponding contributions to the created excited population $N(He^*)$ are proportional to $R_1 \times N(He)$, $R_2 \times N(He^+)$ and $R_3 \times N(He_2^+)$, where $N(He)$, $N(He^+)$ and $N(He_2^+)$ label number densities of the He ground state atoms, ionized helium atoms and ionized helium molecules, respectively. Although the excitation rates R_i ($i = 1, 2, 3$) are mutually comparable (see [41] and references therein), the dominant contribution to $N(He^*)$ comes from electron impact ionization of the ground state atoms because $N(He)$ is order of magnitudes higher than $N(He^+)$ or $N(He_2^+)$. Therefore, in the following considerations we will attribute the creation of the population in the upper level of the 501 nm helium emission line exclusively to the collisions of the fast electrons and ground state He atoms.

The qualitatively different behaviors of He and N_2^+ emission distributions in the jet can be explained in the following manner. The excited He atoms are produced in collision between helium ground state atoms and fast electrons. For instance, to excite the lowest lying He excited state (metastable 2s ^3S state, energy: 19.82 eV) by electron impact, the electron requires velocity of 2.5×10^3 km/s. The measured intensity distributions $I_{501}(x)$ correspond to the number densities $n^*_{He}(x)$ of He atoms excited to the relevant upper state (3^1P^o), which is proportional to the product of fast electron number density $n_e^{fast}(x)$ and the density of the ground-state He atoms $n_{He}(x)$. The $n_{He}(x)$ in the capillary has a constant value n^0_{He} which is defined by the room temperature [38] and atmospheric pressure, while outside the capillary it rapidly decreases. Formally, $n_{He}(x) \propto n^0_{He}\ f(x)$, where $f(x)$ is a function which amounts to 1 in the capillary, monotonously decreases from the capillary orifice and equals to zero for $x = \infty$. Thus, the intensity distributions of early He emission signals can be represented by $I_{501}(x) \propto n^0_{He} f(x)\ n_e^{fast}(x)$. As can be seen in Fig. 3a, the I_{501} intensities in the region near the HV electrode ($8 < x < 11$) are lower than in the jet. The comparison of the latter expression for $I_{501}(x)$ with the measured intensity distributions given in Fig. 3a, implies that the density of fast electrons in the vicinity of the HV electrode (where He density is high and $f(x) = 1$) is smaller than in the plasma jet. The fast electrons are localized in front of the capillary in the region, which is several millimeters long.

As shown previously [38], the formation of N_2^+ ions in the plasma jet produced by the DBD working in filamentary mode is due to comparable contributions of both Penning ionization of nitrogen molecules in collisions with helium metastable atoms ($He^M + N_2 \rightarrow N_2^+ + e^{slow}$) and the charge transfer in collision of ground-state helium ion dimers and nitrogen molecules ($He_2^+ + N_2 \rightarrow N_2^+ + 2He$). However, when DBD is working the homogeneous operation mode, as in the present experiment, the major production of N_2^+ is due to the Penning ionization process [38]. Therefore, the number density of the ionized nitrogen molecules $n^*_{N_2^+}(x)$ is proportional to the product of $n^*_{He}(x) \cdot n_{N_2}(x)$, where $n^*_{He}(x)$ and $n_{N_2}(x)$ are the densities of He metastable atoms and nitrogen molecules in the ground state, respectively. Following the above consideration, the ground state number density of nitrogen $n_{N_2}(x)$ along the x-axis can be represented in the form $n^\infty_{N_2}[1-f(x)]$, where $n^\infty_{N_2}$ is the nitrogen number density in the surrounding air atmosphere (formally: at $x = \infty$). Thus, the distributions of the excited nitrogen ionized molecules can be described by $n^*_{N_2^+}(x) \propto n_e^{fast}(x) f(x)[1-f(x)]$. Note that the shapes of the measured $I_{391}(x)$ distributions are qualitatively in agreement with the product $f(x)[1 - f(x)]$, which equals to zero in the capillary, reaches its maximum at certain position x in the front of the capillary and decreases for large x-values.

The presented measurements show that the spatial and temporal occurrence of the early discharge, *i.e.*, the jet discharge, is in correlation with the early emission signals of the helium lines. This discharge is spatially localized within an effective plasma jet length L_{eff} and temporally within a period of time ΔT. As will be shown in the following, these quantities can be deduced from the data presented in Fig. 3, and in combination with the measured net charges ΔQ they enable the calculation of the average electrical currents in the plasma jet. Similarly to the relationship between the intensities of the coincident emission signals and peak currents in the capillary discharge reported earlier [37], it is plausible to expect that the measured intensities of the early He emission signals should be in direct proportion with the calculated plasma jet currents.

3. Results

We consider the intensity and occurrence time distributions in the plasma jet, *i.e.*, for positions $x > 13$ mm. Here, we define the total intensity of early He emission signals in the jet at particular HV in the form $I^{tot}_{501}(\text{mm a.u.}) = \Delta x \sum_{x=13}^{M} I_{501}(x)$, where M (mm) is the maximum position in the jet at which the intensities were measured, and $\Delta x = 1$ mm is the length increment. We define the effective plasma jet lengths as the ratio of the particular total intensity and maximum intensity I^{max}_{501} measured at $x = 13$: $L_{eff}(\text{mm}) = I^{tot}_{501}/I^{max}_{501}$. In this way, the measured continuously decreasing I_{501} distributions are substituted by rectangular profiles having the height I^{max}_{501} and the length L_{eff}. In that simplified picture, the plasma jet discharge is restricted to the time interval $\Delta T = L_{eff}/v^E_3$, and an average current I_{jet} in that case can be defined as $I_{jet} = \frac{\Delta Q}{\Delta T} = v^E_3\ \Delta Q/L_{eff}$.

The values for the charges Q_N, and Q_P and their differences ΔQ evaluated from the measured currents through capillary at various HV are plotted in Fig. 5a. Fig. 5b shows the excitation velocities v^E_3, which were calculated from the $\tau(x)$ distributions plotted in Fig. 3b. The corresponding effective plasma lengths L_{eff} were calculated from the $I_{501}(x)$ distributions and they are displayed in Fig. 5c. By using the data in Fig. 5, the plasma jet currents I_{jet} were calculated for each value of the applied HV amplitude. The obtained I_{jet} values should be regarded as maximum values, since it is not excluded that the charge ΔQ is partially dissipated along the path between the HV electrode and the capillary orifice. The plasma jet currents are dominantly determined by the values of excitation velocities. Namely, as one can see from Fig. 5a and c, both ΔQ and L_{eff} slightly increase with increasing voltage and their ratio $\Delta Q/L_{eff}$ in the considered voltage range is practically constant and amounts to $(1.6 \pm 0.1) \times 10^{-11}$ C/mm. The obtained I_{jet} values seem to be reasonable in comparison with the currents measured in the capillary. For

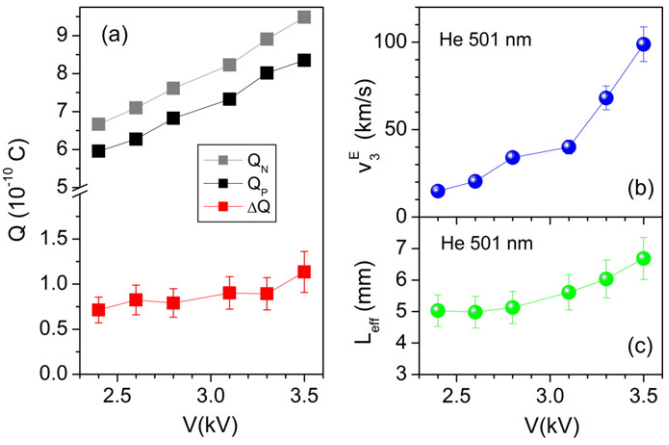

Fig. 5. (a) The values of the charges Q_N, Q_P and their differences ΔQ as a function of the applied HV amplitude. (b) The excitation velocities v_3^E evaluated as the reciprocal slopes of the position-dependent occurrence times given in Fig. 3b. (c) The effective plasma jet lengths L_{eff} calculated from the early He 501 nm emission signals given in Fig. 3a.

instance, at highest HV amplitude of 3.5 kV, the average I_{jet} is defined within the time period $\Delta T \approx 60$ ns and amounts to 1.67 mA. On the other hand, at that voltage, the current corresponding to the negative voltage period, which reflects the total charge transported through the capillary (there is no jet present in the negative HV period), has the full width at half-maximum of 150 ns and the peak value of 6 mA.

In order to find the correlation between the emission intensities and calculated plasma jet currents, the diagram presented in Fig. 6 was constructed. For this purpose, the mean intensity values $I_{501}^{mean} = \sum_{x=13}^{M} I_{501}(x)/(M-13+1)$ were calculated and plotted *versus* calculated values of I_{jet}. Within the error bars, an obvious linear relationship between I_{501}^{mean} (colored symbols) and I_{jet} is present. Qualitatively, the same result can be obtained by plotting the maximum intensities *versus* current, because the mean values for $I_{501}(x)$ distributions are scaled in the same proportions as the corresponding maximum values at $x = 13$. In addition, the normalized maximum intensities of the $I_{391}(x)$ distributions are plotted in Fig. 6. The data are taken from Fig. 4a and, for the sake of the picture clarity, normalized in the manner that the maximum intensity of the N_2^+ 391 emission at 3.5 kV equals to 0.5. These data (circles) also show a clear linear dependence on the calculated values of the plasma jet currents.

As an additional check of the determination of plasma jet currents, the above described procedure was performed using our recent measurements [37] of spatiotemporal behavior of the helium emission intensities at 706 nm at three relatively low HV amplitudes. Presently used capillary DBD was not physically the same as the previous [37], but it was one of the DBDs, which we construct routinely in our laboratory (all with the same geometry), all being nominally the same in the sense of performance and important characteristics. The spatial and temporal distributions of the He 706 nm line [37] are re-plotted here in Fig. 7a and b. The mean values of $I_{706}(x)$ data plotted against the calculated plasma jet currents are shown in Fig. 7c. The linear relationship between the measured line intensities and the calculated plasma jet currents was confirmed, while the currents were one order of magnitude smaller than in the present experiment.

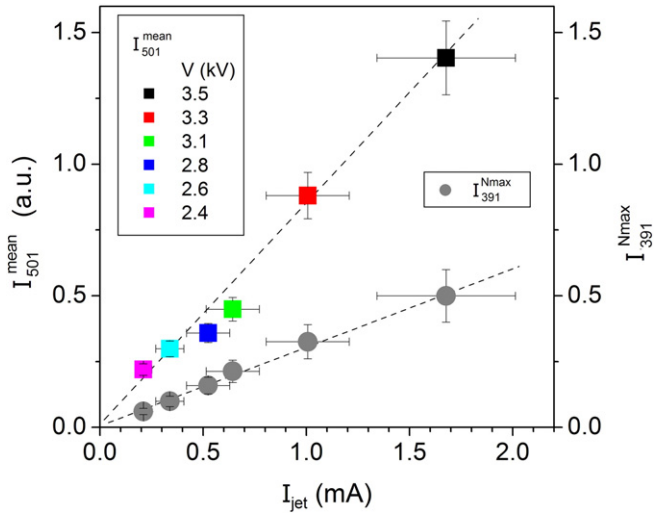

Fig. 6. Relationship between He 501 nm and N_2^+ 391 nm emission intensities measured in the jet and the calculated plasma jet currents. The mean intensities I_{501}^{mean} are related to the $I_{501}(x)$ distributions plotted in Fig. 3a. The I_{391}^{Nmax} data are normalized maximum intensities of the $I_{391}(x)$ distributions displayed in Fig. 4a. See further comments in text.

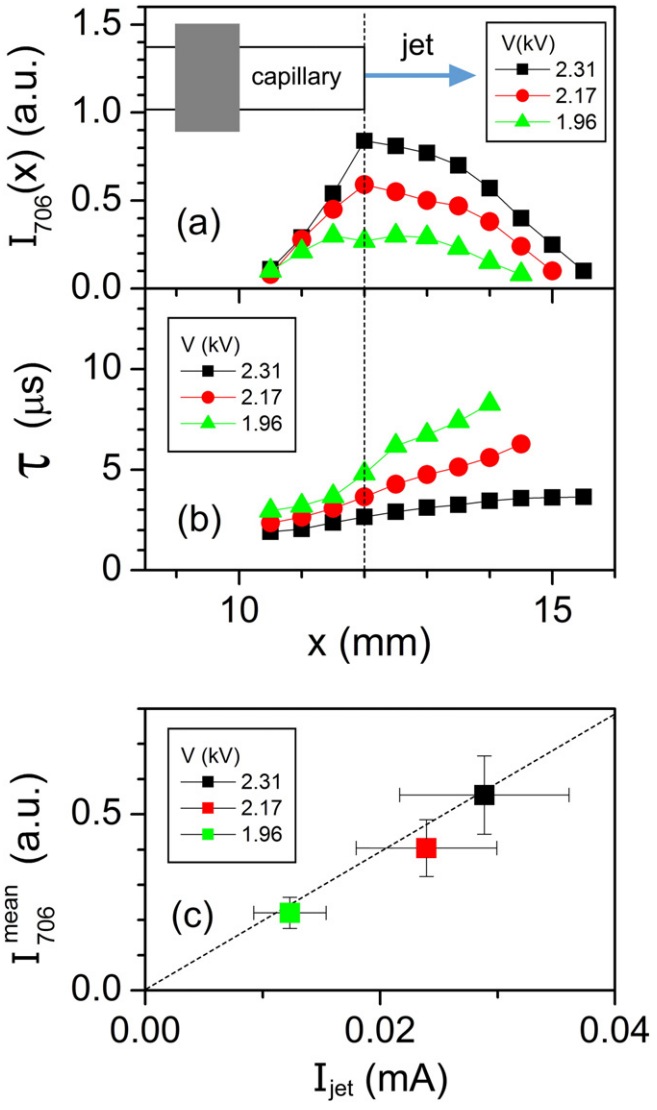

Fig. 7. Relationship between the measured [37] intensities and the calculated plasma jet currents obtained from the spatiotemporal behavior of the He 706 nm line. The measurements [37] were performed at three relatively low HV. (a) Spatial distributions of the intensities of the early He 706 nm signals. (b) Occurrence times corresponding to the measured intensities. (c) The results of the calculations of I_{706}^{mean} dependence on the jet current performed following the procedure described here.

4. Conclusion

Without going into the details of charge dynamics leading to the production of the plasma jet which occurs during the positive HV period and precedes the discharge in the capillary, from the measurements of the capillary discharge currents during the positive and negative period of the square wave HV the resulting charge difference ΔQ can be determined. This charge difference is transported between the positive HV electrode and the ambient atmosphere and leads to the formation of the plasma jet. The investigation of the spatiotemporal behavior of the early He emission line intensities yields the opportunity to define and measure two physical quantities: excitation velocity v^E and effective plasma jet length L_{eff}. The fast electrons producing the excited He atoms are mostly located within the estimated effective plasma jet length. In that region, where helium gas penetrates the air atmosphere, a cascade of de-excitation and excitation processes starting with the formation of ionized nitrogen molecules and establishing the conditions for soft ionization is present. The efficiency of these processes can be put in relation with the plasma jet current which is defined in the form v^E $\Delta Q/L_{eff}$. The results of present measurements yield reliable values for plasma jet currents and linear relationship with the early He line emission intensities over the range of two orders of magnitude.

Acknowledgments

The financial support by the Ministerium für Innovation, the Wissenschaft und Forschung des Landes Nordrhein-Westfalen, the Bundesministerium für Bildung und Forschung, the Deutsche Forschungsgemeinschaft (project no. FR 1192/13-1) is gratefully acknowledged. This work has been supported in part by the Croatian Science Foundation under the project no. 2753.

References

[1] K. Kunze, M. Miclea, G. Musa, J. Franzke, C. Vadla, K. Niemax, Diode laser-aided diagnostics of a low-pressure dielectric barrier discharge applied in element-selective detection of molecular species, Spectrochim. Acta Part B 57 (2002) 137–146.
[2] J. Hu, W. Li, C. Zheng, X. Hou, Dielectric barrier discharge in analytical spectrometry, Appl. Spectrosc. Rev. 46 (2011) 368–387.
[3] C. Guo, F. Tang, J. Chen, X. Wang, S. Zhang, X. Zhang, Development of dielectric-barrier-discharge ionization, Anal. Bioanal. Chem. 407 (2015) 2345–2364.
[4] C. Meyer, S. Müller, E.L. Gurevich, J. Franzke, Dielectric barrier discharges in analytical chemistry, Analyst 136 (2011) 2427–2440.
[5] H. Hayen, A. Michels, J. Franzke, Dielectric barrier discharge ionization for liquid chromatography/mass spectrometry, Anal. Chem. 81 (2009) 10239–10245.
[6] N. Na, M. Zhao, S. Zhang, C. Yang, X. Zhang, Development of a dielectric barrier discharge ion source for ambient mass spectrometry, J. Am. Soc. Mass Spectrom. 18 (2007) 1859–1862.
[7] B. Gilbert-López, J.F. García-Reyes, C. Meyer, A. Michels, J. Franzke, A. Molina-Díaz, H. Hayen, Simultaneous testing of multiclass organic contaminants in food and environment by liquid chromatography/dielectric barrier discharge ionization-mass spectrometry, Analyst 137 (2012) 5403–5410.
[8] B. Gilbert-López, M. Schilling, N. Ahlmann, A. Michels, H. Hayen, A. Molina-Díaz, J.F. García-Reyes, J. Franzke, Ambient diode laser desorption dielectric barrier discharge ionization mass spectrometry of nonvolatile chemicals, Anal. Chem. 85 (2013) 3174–3182.
[9] R. Gras, J. Luong, M. Monagle, B. Winniford, Gas chromatographic applications with the dielectric barrier discharge detector, J. Chromatogr. Sci. 44 (2006) 101–107.
[10] Y. He, Y. Lv, Y. Li, H. Tang, L. Li, X. Wu, X. Hou, Dielectric barrier discharge-induced chemiluminescence: potential application as GC detector, Anal. Chem. 79 (2007) 4674–4680.
[11] S.B. Olenici-Craciunescu, A. Michels, C. Meyer, R. Heming, S. Tombrink, W. Vautz, J. Franzke, Characterization of a capillary dielectric barrier plasma jet for use as a soft ionization source by optical emission and ion mobility spectrometry, Spectrochim. Acta Part B 64 (2009) 1253–1258.
[12] A. Michels, S. Tombrink, W. Vautz, M. Miclea, J. Franzke, Spectroscopic characterization of a microplasma used as ionization source for ion mobility spectrometry, Spectrochim. Acta Part B 62 (2007) 1208–1215.
[13] Z. Zhu, J. Liu, S. Zhang, X. Na, X. Zhang, Determination of Se, Pb, and Sb by atomic fluorescence spectrometry using a new flameless, dielectric barrier discharge atomizer, Spectrochim. Acta Part B 63 (2008) 431–436.
[14] M. Miclea, K. Kunze, G. Musa, J. Franzke, K. Niemax, The dielectric barrier discharge — a powerful microchip plasma for diode laser spectrometry, Spectrochim. Acta Part B 56 (2001) 37–43.
[15] D.R. Ifa, A.U. Jackson, G. Paglia, R.G. Cooks, Forensic applications of ambient ionization mass spectrometry, Anal. Bioanal. Chem. 394 (2009) 1995–2008.
[16] N. Na, C. Zhang, M. Zhao, S. Zhang, C. Yang, X. Fang, X. Zhang, Direct detection of explosives on solid surfaces by mass spectrometry with an ambient ion source based on dielectric barrier discharge, J. Mass Spectrom. 42 (2007) 1079–1085.
[17] S. Tümmel, N. Mertens, J. Wang, W. Viöl, Low temperature plasma treatment of living human cells, Plasma Process. Polym. 4 (2007) S465–S469.
[18] G.E. Morfill, T. Shimizu, B. Steffes, H.-U. Schmidt, Nosocomial infections — a new approach towards preventive medicine using plasmas, New J. Phys. 11 (2009) 115019(1)–115019(10).
[19] G. Fridman, G. Friedman, A. Gutsol, A.B. Shekhter, V.N. Vasilets, A. Fridman, Applied plasma medicine, Plasma Process. Polym. 5 (2008) 503–533.
[20] K. Pochner, W. Neff, R. Lebert, Atmospheric pressure gas discharges for surface treatment, Surf. Coat. Technol. 74–75 (1995) 394–398.
[21] G. Baravian, D. Chaleix, P. Choquet, P.L. Nauche, V. Puech, M. Rozoy, Oil removal from iron surfaces by atmospheric-pressure barrier discharges, Surf. Coat. Technol. 115 (1999) 66–69.
[22] M.A. Malik, A. Ghaffar, S.A. Malik, Water purification by electrical discharges, Plasma Sources Sci. Technol. 10 (2001) 82–91.
[23] O. Goossens, E. Dekempeneer, D. Vangeneugden, R. Van de Leest, C. Leys, Application of atmospheric pressure dielectric barrier discharges in deposition, cleaning and activation, Surf. Coat. Technol. 142 (2001) 474–481.
[24] B. Gilbert-López, H. Geltenpoth, C. Meyer, A. Michels, H. Hayen, A. Molina-Díaz, J.F. García-Reyes, J. Franzke, Performance of dielectric barrier discharge ionization mass spectrometry for pesticide testing: a comparison with atmospheric pressure chemical ionization and electrospray ionization, Rapid Commun. Mass Spectrom. 27 (2013) 419–429.
[25] I.P. Vinogradov, K. Wiesemann, Classical absorption and emission spectroscopy of barrier discharges in N_2/NO and O_2/NO_x mixtures, Plasma Sources Sci. Technol. 6 (1997) 307–316.
[26] T.I. Lee, K.W. Park, H.K. Baik, S.M. Lee, Dielectric barrier hollow cathode discharge and its enhanced performance for light source, Appl. Phys. Lett. 87 (2005) 261502(1)–261502(3).
[27] Y. Yu, Z. Du, M. Chen, J. Wang, Atmospheric-pressure dielectric-barrier discharge as a radiation source for optical emission spectrometry, Angew. Chem. Int. Ed. 47 (2008) 7909–7912.
[28] Z.L. Zhu, G.C.Y. Chan, S.J. Ray, X.R. Zhang, G.M. Hieftje, Microplasma source based on a dielectric barrier discharge for the determination of mercury by atomic emission spectrometry, Anal. Chem. 80 (2008) 8622–8627.
[29] X. Lu, M. Laroussi, Dynamics of an atmospheric pressure plasma plume generated by submicrosecond voltage pulses, J. Appl. Phys. 100 (2006) 063302 (1)–063302 (6) 20.
[30] N. Jiang, A. Ji, Z. Cao, Atmospheric pressure plasma jet: effect of electrode configuration, discharge behavior, and its formation mechanism, J. Appl. Phys. 106 (2009) 013308(1)–013308(7).
[31] K. Urabe, T. Morita, K. Tachibana, B.N. Ganguly, Investigation of discharge mechanisms in helium plasma jet at atmospheric pressure by laser spectroscopic measurements, J. Phys. D. Appl. Phys. 43 (2010) 095201(1)–095201(13).
[32] B.L. Sands, R.J. Leiweke, B.N. Ganguly, Spatiotemporally resolved Ar (1s5) metastable measurements in a streamer-like He/Ar atmospheric pressure plasma jet, J. Phys. D. Appl. Phys. 43 (2010) 282001(1)–282001(5).
[33] J.-P. Boeuf, L.L. Yang, L.C. Pitchford, Dynamics of a guided streamer ('plasma bullet') in a helium jet in air at atmospheric pressure, J. Phys. D. Appl. Phys. 46 (2013) 015201(1)–015201(13).
[34] E. Karakas, M.A. Akman, M. Laroussi, The evolution of atmospheric-pressure low-temperature plasma jets: jet current measurements, Plasma Sources Sci. Technol. 21 (2012) 034016(1)–034016(10).
[35] B.L. Sands, B.N. Ganguly, K. Tachibana, A streamer-like atmospheric pressure plasma jet, Appl. Phys. Lett. 92 (2008) 151503(1)–151503(3).
[36] V. Horvatic, A. Michels, N. Ahlmann, G. Jestel, D. Veza, C. Vadla, J. Franzke, Time- and spatially-resolved emission spectroscopy of the dielectric barrier discharge for soft ionization sustained by a quasi-sinusoidal high voltage, Anal. Bioanal. Chem. 407 (2015) 6689–6696.
[37] V. Horvatic, A. Michels, N. Ahlmann, G. Jestel, D. Veza, C. Vadla, J. Franzke, Time-resolved spectroscopy of a homogeneous dielectric barrier discharge for soft ionization driven by square-wave high voltage, Anal. Bioanal. Chem. DOI 10.1007/s00216-015-8969-7.
[38] S. Müller, T. Krähling, D. Veza, V. Horvatic, C. Vadla, J. Franzke, Operation modes of the helium dielectric barrier discharge for soft ionization, Spectrochim. Acta Part B 85 (2013) 104–111.
[39] C. Meyer, S. Müller, B. Gilbert-López, J. Franzke, Impact of homogeneous and filamentary discharge modes on the efficiency of dielectric barrier discharge ionization mass spectrometry, Anal. Bioanal. Chem. 405 (2013) 4729–4735.
[40] V. Horvatic, C. Vadla, J. Franzke, Discussion of fundamental processes in dielectric barrier discharges used for soft ionization, Spectrochim. Acta Part B 100 (2014) 52–61.
[41] T. Martens, A. Bogaerts, W. Brok, J. van Dijk, Computer simulations of a dielectric barrier discharge used for analytical spectrometry, Anal. Bioanal. Chem. 388 (2007) 1583–1594.